Plasma Phys. Control. Fusion **42** (2000) 41–56. Printed in the UK PII: S0741-3335(00)05408-7

Discharge modes and wave structures using loop antennae in a helicon plasma source

Shunjiro Shinohara and Kenji Yonekura

Interdisciplinary Graduate School of Engineering Sciences, Kyushu University, Kasuga, Fukuoka 816-8580, Japan

E-mail: sinohara@aees.kyushu-u.ac.jp

Received 22 June 1999, in final form 2 November 1999

Abstract. Discharge modes separated by density jumps in a helicon plasma source were controlled successfully by changing the antenna wavenumber spectrum with a two-loop antenna, in addition to varying the filling pressure P and the magnetic field B. For the case of wave excitation with the anti-parallel antenna current direction, the threshold power $P_{\rm th}$ for a density jump, regardless of B and P, was larger than in the case of a parallel direction, and $P_{\rm th}$ became larger with the increase in B in both cases. From the excited wave structures, it was found that the helicon wave plasma was observed after the jump with the high field, while with the low field regardless of the density region or with the high field before the jump, an inductively coupled plasma was found. No indication of a major role of the lower hybrid wave and Trivelpiece–Gould wave on the plasma production was observed.

1. Introduction

Methods of efficiently producing plasmas with high electron density $n_{\rm e}$ at low filling pressure are urgently required for many applications, such as plasma processing and confinement devices. A helicon wave source with $n_{\rm e}$ up to the order of 10^{13} cm^{-3} [1–4] is a very attractive proposal, and many empirical and theoretical characterizations of this wave, as well as extensive investigations of the plasma performance have been carried out, with the diameter ranging from several centimetres to several tens of centimetres [5–34].

However, due to some difficulties in making temporally and spatially resolved measurements, such as reducing radio frequency (RF) noise, there still remains an open question to be answered as for the production mechanism. Proposed candidates are electron Landau damping [2, 5, 6, 14, 30] (electron beams are important but this damping was discarded recently by Chen and Blackwell [34]), collisional damping [2, 5, 6, 10, 15], presence of the lower hybrid (LH) wave [26–28] (this wave is considered to alleviate plasma production) and the Trivelpiece–Gould (TG) wave with short wavelength [19, 21, 22, 24, 31–34] (theoretically, TG waves exist in the low field and low density regions or mode conversion from the helicon wave to the TG wave may be important).

Therefore, identifying this physically interesting but probably complicated mechanism is important in order to understand and control the plasma behaviour in this promising source. To understand this mechanism, we must consider the nonlinear, hysteresis behaviour of the so-called 'density jump' (see examples in [7, 12, 18, 29]), which is observed between the discharge modes from lower to higher densities in this source. This jump is characterized as a steep,

0741-3335/00/010041+16$30.00 © 2000 IOP Publishing Ltd

abrupt increase in the density within a time scale shorter than several hundreds of microseconds, and occurs above certain threshold values of the RF power and filling pressure. The sudden transition may be a clue for the total understanding, in the future, of the helicon wave produced plasma source from the plasma generation to sustainment phases. Note that this jump is considered to be a universal plasma phenomenon, which is found in, for example, DC [35], inductively coupled plasma (ICP) [36] and RF plasma discharges in fusion devices [37].

In previous work [12, 16, 17, 23, 29], we have demonstrated that the helicon wave was observed after the density jump and carried a considerable part of the injected RF power. This conclusion was made from a detailed analysis of the excited wave structures. In the most recent work, the discharge regime was changed by the initial trial of controlling the antenna wavenumber spectrum [29], and the results were compared with ICP discharges,which have no magnetic field.

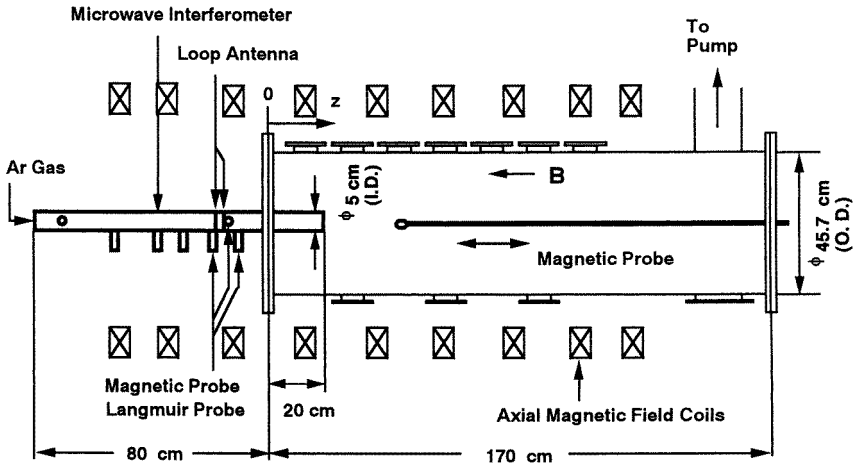

Figure 1. Schematic view of the experimental apparatus.

In this paper, we successfully demonstrate the control of the discharge regimes by considering the importance of exciting the component of high or low wavenumbers. A two-loop antenna, with parallel or anti-parallel RF current directions, were used in a wide range of magnetic fields (0 G $\leqslant B \leqslant$ 1000 G) for two argon gas pressures ($P = 6$ and 51 mTorr). Furthermore, in the individual regimes, the dispersion relation and wave structures were investigated, which led to the conclusion that after the jump with the low field or before the density jump regardless of the field, ICP (or capacitively coupled plasma (CCP) [36] in the lower density region) was produced. On the other hand, after the jump with the high field, only the helicon wave plasma was observed. No major contributions from other waves, such as LH and TG waves, were suggested in our experiments.

This paper is organized as follows. In sections 2 and 3, the experimental set-up and the dispersion relation for our experimental conditions are described, respectively. Results of the plasma performance and the excited wave structures considering the helicon and TG wave dispersions are presented in section 4. Finally, section 5 contains conclusions.

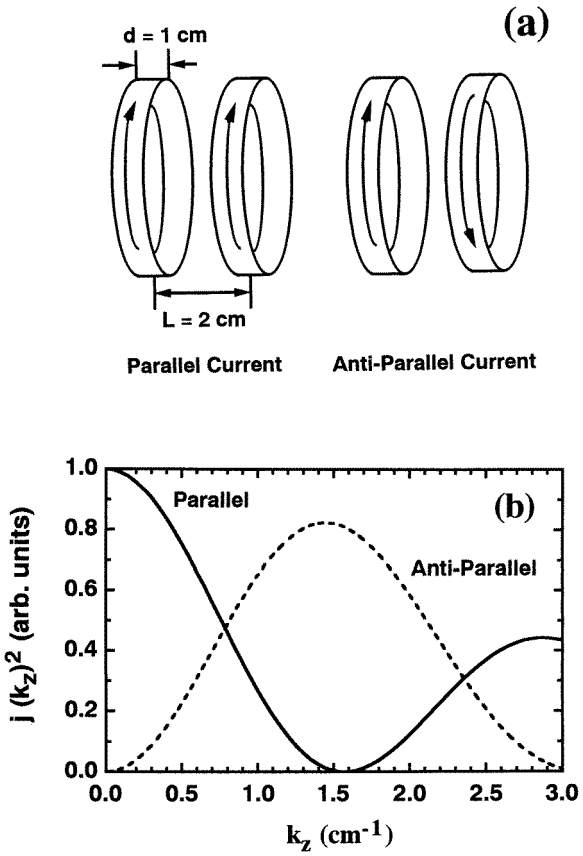

Figure 2. (a) Antenna structures using two loops (parallel and anti-parallel antenna currents) and (b) power spectra of antenna wavenumber $j\,(k_z)^2$ for both antenna configurations.

2. Experimental set-up

The experimental system is shown in figure 1. The Ar gas was fed into the left-hand side of the Pyrex tube (5 cm inner diameter and 100 cm total length), which was connected to the vacuum chamber (45.7 cm outer diameter and 170 cm length). An axial magnetic field was applied. The RF frequency f and power were 7 MHz and <5 kW, respectively, and the power was pulsed with a 2 ms width and a duty cycle of 1/16 to prevent thermal damage to the antenna. The RF power supply was connected to the antenna through a directional coupler, which picks up the incident and reflected power, a matching box and monitors for the antenna's voltage and current. Plasma parameters (typical electron temperature T_e of 4–8 eV in a wide range of $n_e = 10^9$–6×10^{13} cm^{-3}) and excited wave fields were measured by movable Langmuir (0.1 cm radius with 0.3 cm length) and magnetic (one-turn loop with 0.5 cm diameter) probes inserted into the plasma. n_e was calibrated by the 70 GHz interferometer.

The width d of each loop (made of copper, 0.03 cm thick, which was wound around the tube), was 1 cm separated by $L = 2$ cm, as shown in figure 2(a). In the case of the parallel (anti-parallel) antenna current direction, the first peak (zero) point of the power spectrum $j\ (k_z)^2$ using an antenna current of is at the parallel wavenumber $k_z = 0$ cm^{-1} (0 cm^{-1}) and reaches

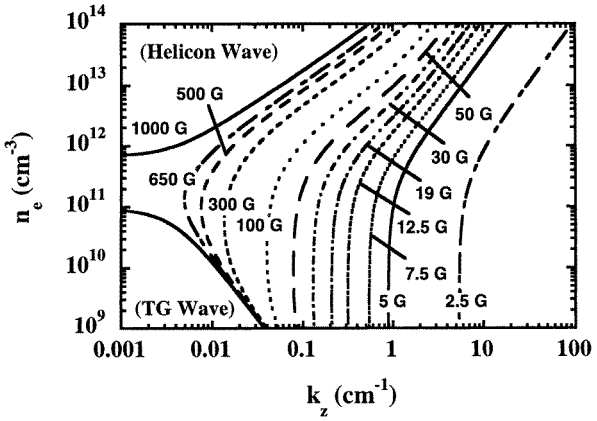

Figure 3. Electron density n_e as a function of parallel wavenumber k_z under different magnetic fields with azimuthal mode number $m = 0$, the first radial mode and frequency $f = 7$ MHz (calculation).

zero (peak) value at 1.6 cm^{-1} (1.4 cm^{-1}) (see figure 2(b)). Here, the assumption of a uniform profile of the RF current in the antenna was confirmed in a previous experiment [29].

3. Dispersion relation

We use the cold-plasma approximation [38] to calculate the dispersion relation for our experimental conditions. Note that the calculation results hold in all the density regions and for different magnetic fields. Figure 3 shows the dependence of n_e on k_z for different magnetic fields. For this calculation, we used the azimuthal mode number $m = 0$ [2] and $f = 7$ MHz with the first radial mode (plasma radius $a = 2.5$ cm), i.e. the perpendicular wavenumber $k_{perp} = 3.8/a = 1.5$ cm^{-1}. From this figure, it can be seen that above the field B_{LH}, at which f is equal to the lower hybrid frequency f_{LH}, there is a density gap. The density changes from 9.4×10^{10} to 6.8×10^{11} cm^{-3} at $B = 1000$ G. B_{LH} is about 680 G and f_{LH} can be expressed approximately as the square root of the product of the electron and ion cyclotron frequencies. With the high field greater than ~100 G, the increase in n_e causes k_z to decrease (increase) in the lower (higher) density region of the TG (helicon) wave excitation with a fixed value of k_{perp} (see figures 4 and 5 to distinguish the TG wave with the high k_{perp} value from the helicon wave with the low value). For the case of the low field (less than ~100 G) and low density, k_z is weakly dependent on n_e. Typically, after the density jump to $n_e = 10^{13}$ cm^{-3}, k_z values of 6.0, 1.5, 0.2 and 0.057 cm^{-1} are required at $B = 5$, 30, 300 and 1000 G, respectively. From figures 2 and 3, the configuration of the two loops with parallel (anti-parallel) antenna currents is considered to be favourable to excite the helicon (TG) wave under the high (low) field. When the second radial mode ($k_{perp} = 7.0/a = 2.8$ cm^{-1}) is used instead of the first, the dispersion curve in figure 3 extends right (left) in the lower (higher) density region, and the density gap at $B > B_{LH}$ becomes larger (see figure 13). In summary, as far as the low radial mode is concerned, the helicon (TG) wave can be excited in the high (low) density region, but we must note that a low k_z value, for example <0.1 cm^{-1} (wavelength $\lambda > 63$ cm), is unrealistic in the experiment since the excited λ is comparable to or larger than the axial plasma size.

When the proper values of k_z and n_e are chosen, with $B < B_{LH}$, we obtain the lower and higher k_{perp} values, corresponding to the helicon and TG waves, respectively, as shown

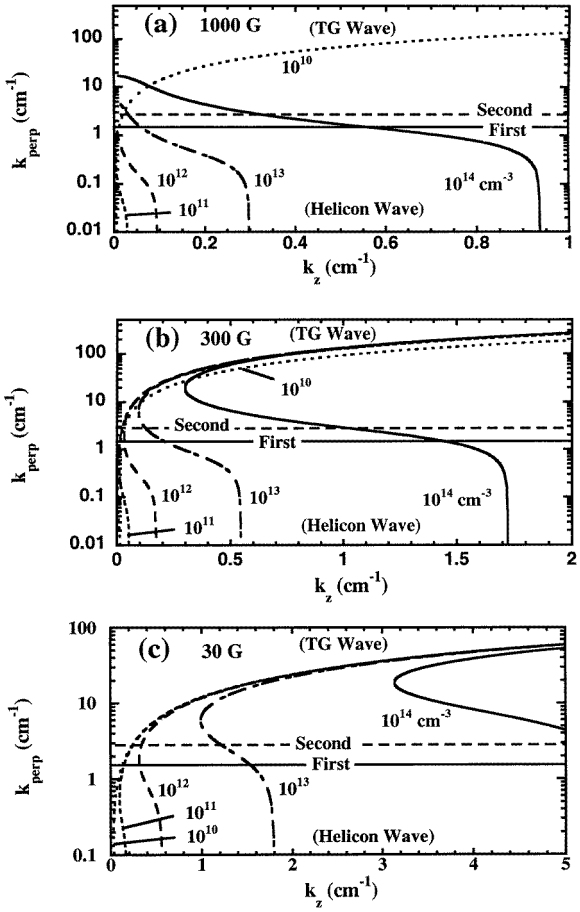

Figure 4. Relationship between perpendicular wavenumber k_{perp} and parallel wavenumber k_z under different electron densities with magnetic field B equal to (a) 1000 G, (b) 300 G and (c) 30 G at frequency f of 7 MHz (calculation).

in figure 4. However, only one solution of k_{perp}, typically a helicon wave, can be found at $B > B_{\mathrm{LH}}$, for example, when n_{e} is higher than several times 10^{11} cm^{-3}, with $B = 1000$ G (see figures 3 and 4(a)). On the other hand, at low B and low n_{e}, only the TG wave can exist if k_{perp} is larger than the value obtained with the first radial mode. Figure 5 shows the relationship between k_{perp} and n_{e} for a fixed value of k_z. It can again be seen that the TG (helicon) wave exists in the low (high) density region with a higher (lower) k_{perp} value, and a higher value of k_{perp} is obtained when the value of n_{e} is fixed and k_z is increased. For the case of $B < B_{\mathrm{LH}}$, a smooth connection between the helicon and TG waves is observed, which can be expected to play a part in direct mode conversions.

So far, a uniform density profile has been assumed in deriving the dispersion relation. Density peaking causes a decrease in k_z for a fixed n_{e} value in the helicon wave ($m = 0$ mode) from calculations [7]. This is understood to mean that the larger effective k_{perp} value (in other words, contraction of the plasma radius) is equivalent to density peaking [9]. As was mentioned above, the dispersion curve extends right (left) in the lower (higher) density region with the higher k_{perp} value (see figure 13).

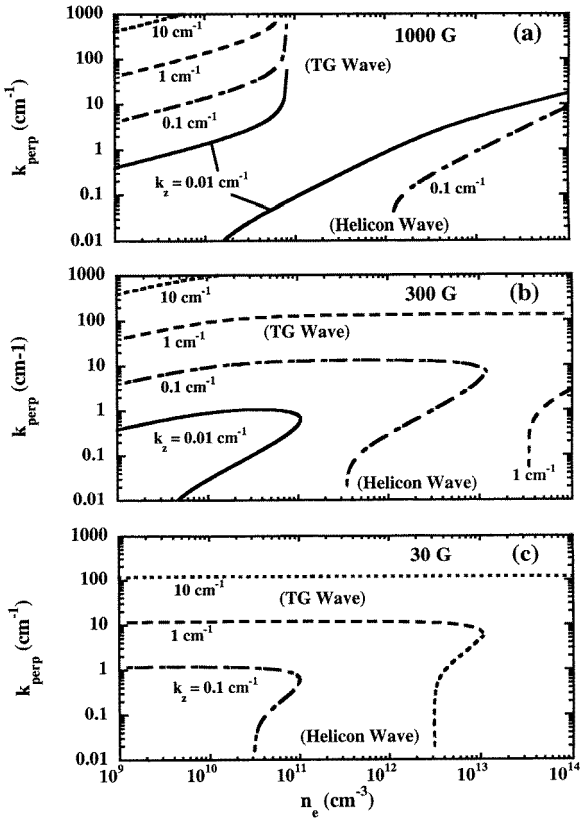

Figure 5. Relationship between perpendicular wavenumber k_{perp} and electron density n_{e} under different parallel wavenumbers with the magnetic field B equal to (a) 1000 G, (b) 300 G and (c) 30 G at frequency f of 7 MHz (calculation).

4. Experimental results

Figure 6 shows the relationship between n_{e} and the input power P_{in} (the difference between the incident and reflected power), for two cases (parallel and anti-parallel RF current directions) at $P = 6$ and 51 mTorr and for B in the range of 30–1000 G. n_{e} was measured in the centre of the tube at an axial distance of 0.5 cm from the edge of the antenna and no large change along the axial direction was observed [29]. At $P = 6$ mTorr, there were density jumps as P_{in} increased, and the threshold power, P_{th}, for jumps became larger with the increase in B. However, P_{th} was smaller at $B = 1000$ G than at $B = 650$ G. The n_{e} change in this jump at $P = 6$ mTorr (figure 6(a)) was somewhat smaller than at $P = 51$ mTorr (figures 6(b) and (c)), and the reason why the second density jump from 10^{11} to 10^{12} cm^{-3} ranges with $B = 100$ G was mild at $P = 6$ mTorr might be due to the difficulty in the tuning of the impedance matching. The first jumps, with $B = 30$, 50 and 100 G at this pressure, from $n_{\mathrm{e}} = 10^{10}$ to 10^{11}–10^{12} cm^{-3} ranges and $P_{\mathrm{th}} < 200$ W, are considered to be the transitions from CCP to ICP modes, and jumps with $B = 100$–1000 G, from 10^{11} to 10^{12}–10^{13} cm^{-3} ranges, are from the ICP to helicon wave modes. These wave structures will be described later and the three modes of CCP, ICP and helicon are similar to those described in [18]. For the case of the anti-parallel antenna current direction at $P = 6$ mTorr, the plasma was not initiated in all the regions of B and P_{in}, which

is consistent with previous results [29].

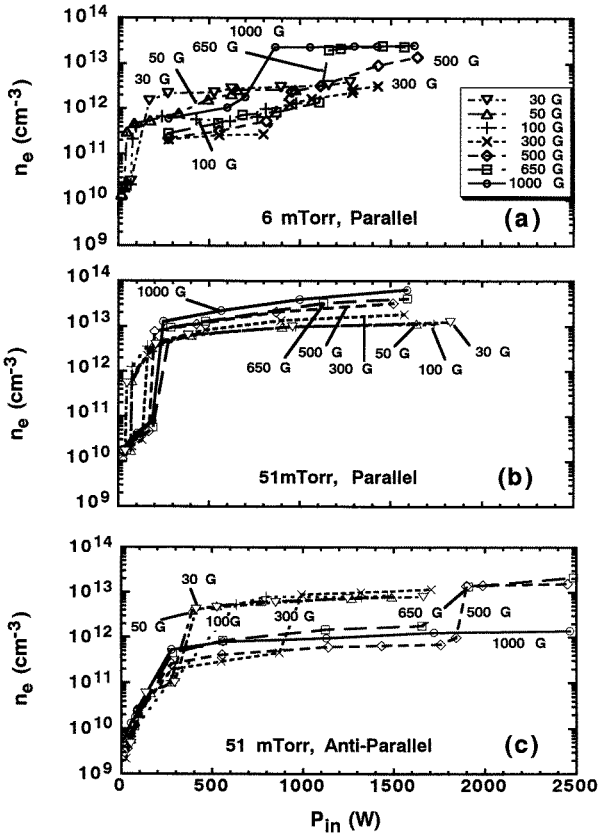

Figure 6. Dependence of electron density n_e on input RF power P_{in} under different magnetic fields ($B \geqslant 30$ G) with (a) parallel (pressure $P = 6$ mTorr), (b) parallel ($P = 51$ mTorr) and (c) anti-parallel ($P = 51$ mTorr) antenna current directions.

At $P = 51$ mTorr, for both antenna current directions, density jumps became clearer and had the same behaviour as in the case of $P = 6$ mTorr with parallel current: P_{th} increased with the increase in B, but for the parallel current case with $P = 51$ mTorr, $P_{th} < 300$ W was lower than for the anti-parallel current. At $B = 1000$ G, no density jump was observed even at the high power of $P_{in} = 2500$ W (figure 6(c)). This mode of operation is useful to control n_e continuously, as desired in many plasma applications. Before the main density jump to $\sim 10^{13}$ cm^{-3}, a small increase in n_e was observed (mainly in the ICP mode) with $P_{in} < 200$–300 W. Figure 7 shows the same plots as in figure 6 for low fields ($B < 20$ G) at $P = 51$ mTorr. The dependence of n_e on P_{in} did not change with B (down to no field), but P_{th} for the $n_e \sim 10^{10}$ to $\leqslant 10^{13}$ cm^{-3} jump, which is considered to be the jump from CCP to ICP modes, was again much lower for the parallel antenna current ($\sim$40 W) than for the anti-parallel current ($\sim$300 W). For the case of the parallel antenna current at $P = 6$ mTorr with $B < 20$ G, P_{th} was much smaller than 300 W. The fact that P_{th} was lower for the case of the parallel current having a low wavenumber component than for the case of the anti-parallel current having a high wavenumber component, can be explained as follows. For the parallel case, we can expect easier matching between wavenumbers in the antenna spectra and in the plasma, determined by the helicon wave dispersion (see discussions on the spectrum above,

and figures 2–5), and the non-cancellation of the excited electric field between loops [39].

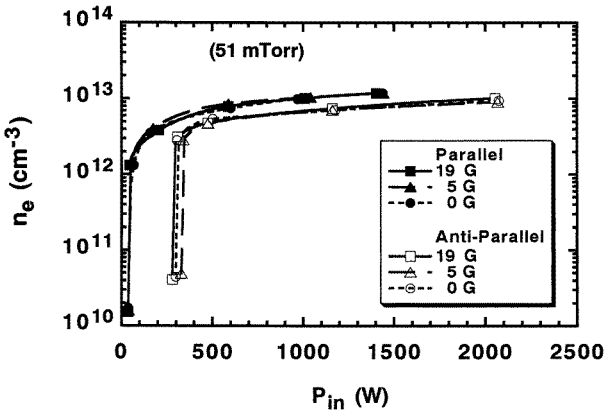

Figure 7. Dependence of electron density n_e on input power P_{in} under different magnetic fields ($B < 20$ G) with parallel and anti-parallel antenna current directions ($P = 51$ mTorr).

Figures 8 and 9 show the total loading resistance $R_p + R_c$ as a function of P_{in} at $P = 51$ mTorr, for both antenna current directions, and for high ($\geqslant$30 G) and low ($<$20 G) magnetic fields, respectively. Here, R_c (0.4–0.5 Ω) and R_p indicate the vacuum (i.e. circuit loss) and plasma loading resistances, respectively [39]. In this expression, the antenna loading ($=P_{in}$ divided by the square of the effective antenna current) is expressed as $R_p + R_c$ (R_c) in the presence (absence) of the plasma, and the power coupling efficiency can be defined as $R_p/(R_p + R_c)$. This loading is a measure of the wave coupling to the plasma and is useful for estimating the power balance. From these figures, the jumps in the resistance corresponded well with the density jumps (i.e. they occurred at $P = P_{th}$), and the total loading after the jump was larger for the case of the parallel antenna current than for the anti-parallel current, regardless of B. In the low field regions, less than 100 G, the dependence of antenna loading on the RF power did not change very much with the change in the field. The present results for the loading resistance and P_{th} are consistent with the analytical results [22] in that the resistance decreases rapidly with k_z, and are also in good agreement with the calculation results [20], showing the maximum resistance at the low k_z value.

As shown in figures 6 and 10, there were no appreciable changes in P_{th} and n_e, including radial density profiles, around the region of f_{LH}. We also changed B from 650 to 690 G in this region to check these parameters in more detail. However, no clear indication of the role of the LH wave was found, whereas some groups [26–28] have claimed that P_{th} (n_e) was lower (higher) around $f \sim f_{LH}$ at a lower pressure than used here. Note that even if the LH wave plays some role in plasma production, it does not contribute to the main production since the high n_e plasma can be generated over a wide range of magnetic fields, regardless of the value of B_{LH} (see figure 6). Figure 10 shows that the density profile at $P = 6$ mTorr became peaked (broad) in the high density region of greater than 10^{12} cm^{-3} compared with the profile in the low density region of $\sim 10^{10}$ cm^{-3} under the high (low) magnetic field, mainly due to the effect of the helicon wave propagation (shielding effect on the electric field in the ICP mode). With both antenna current directions at $P = 51$ mTorr, changes in density profiles from low to high densities were smaller with the high magnetic field, whereas broadening of the profile was found with the low magnetic field.

Next we will present results on the excited wave structures. Figure 11 shows an

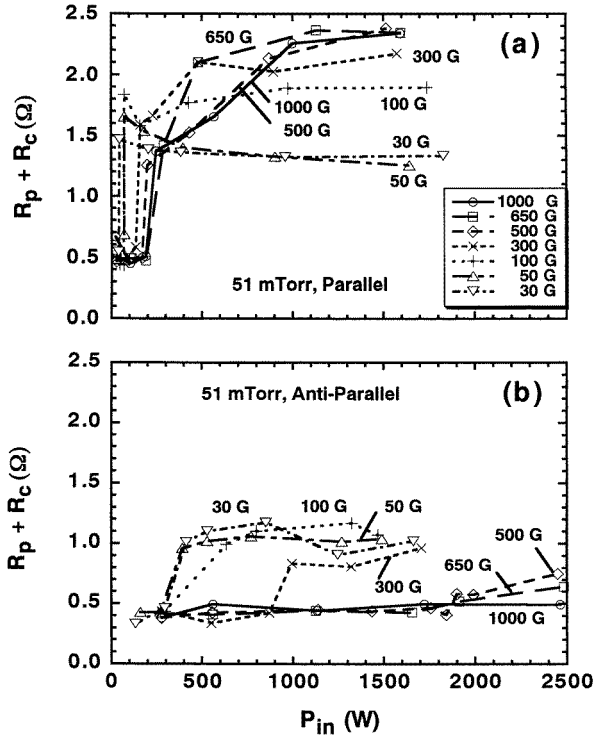

Figure 8. Total antenna loading resistance $R_p + R_c$ as a function of input power P_{in} under different magnetic fields ($B \geqslant 30$ G) with (a) parallel and (b) anti-parallel antenna current directions ($P = 51$ mTorr).

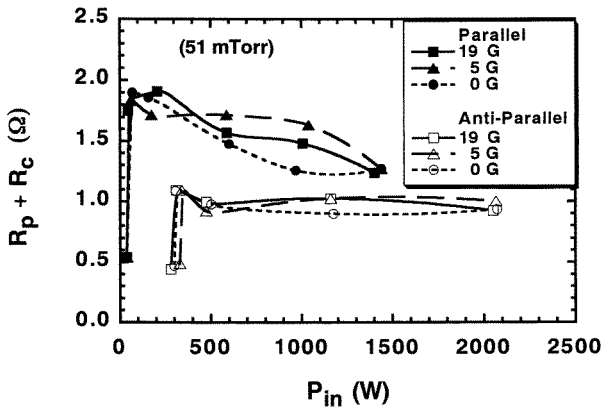

Figure 9. Total antenna loading resistance $R_p + R_c$ as a function of input power P_{in} under different magnetic fields ($B < 20$ G) with parallel and anti-parallel antenna current directions ($P = 51$ mTorr).

example of the axial profiles of the excited magnetic fields B_z (axial component) in the low ($\sim 2 \times 10^{11}$ cm^{-3}) and high ($\sim 10^{13}$ cm^{-3}) density regions. Profiles for different wave phases are shown. The plasma conditions were an anti-parallel current with $B = 300$ G and

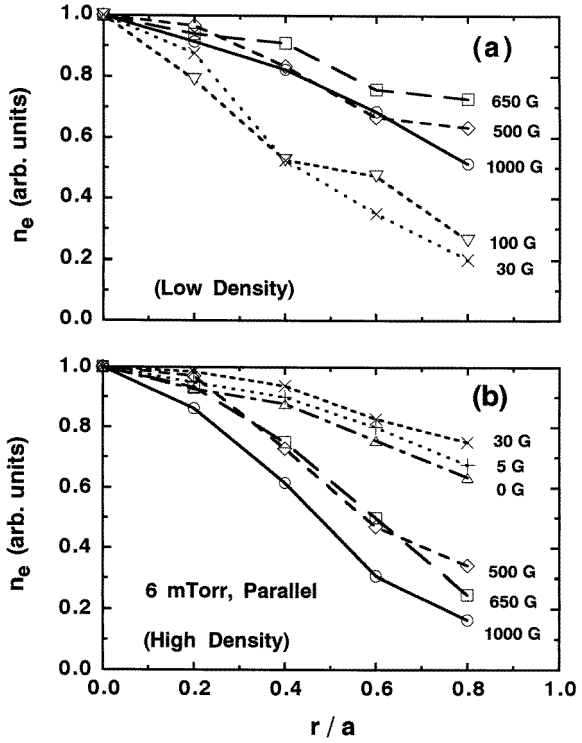

Figure 10. Normalized electron density profiles in the radial direction under different magnetic fields in (a) low and (b) high density regions (parallel antenna current at $P = 6$ mTorr).

$P = 51$ mTorr. Here, $z = 0$ cm is defined at the inner left surface of the vacuum chamber, 20 cm from the right edge of the Pyrex tube (see figure 1). Before the density jump (figure 11(a)), the standing waves existed near the antenna, but propagating waves to the right and left of the antenna region were observed after the jump (figure 11(b)). When the field was more than several tens of G after the jump, wave propagation was observed and the k_z value decreased with the increase in B without a large change in n_e, which is consistent with the dispersion relation. The reason why the region of wave propagation is narrow (about 40 cm in axial length) is mainly because of the high P (51 mTorr) and high n_e, causing strong collisional wave damping. If the wavelength of the helicon wave needs to be less than the axial length of the excited wave region, higher n_e, and thus higher P_{th}, are required with the increase in B from the dispersion, as shown in figures 3–5, which could explain the results in figure 6 after the jump. On the other hand, with the same P_{in} after the jump, the k_z value is considered to become smaller with higher B, which is consistent with the results in figure 12, since there were no large differences in the value of n_e after the jump (see figure 6).

Figure 12 shows the experimentally obtained dependence of n_e/B on k_z, after the jump, for the different B values, with $P_{in} \sim 2000$ W and $P = 51$ mTorr. Most of the data agreed well with the theoretical curve of the helicon wave (the first radial mode with $m = 0$), regardless of P, antenna current direction and the radius in the measurements. There was a tendency for k_z to decrease with the increase in B, especially for the anti-parallel case. This supports the above discussion that in the case of the anti-parallel current, which has a low fraction of the low wavenumber component, high RF power is needed in order that high density is reached.

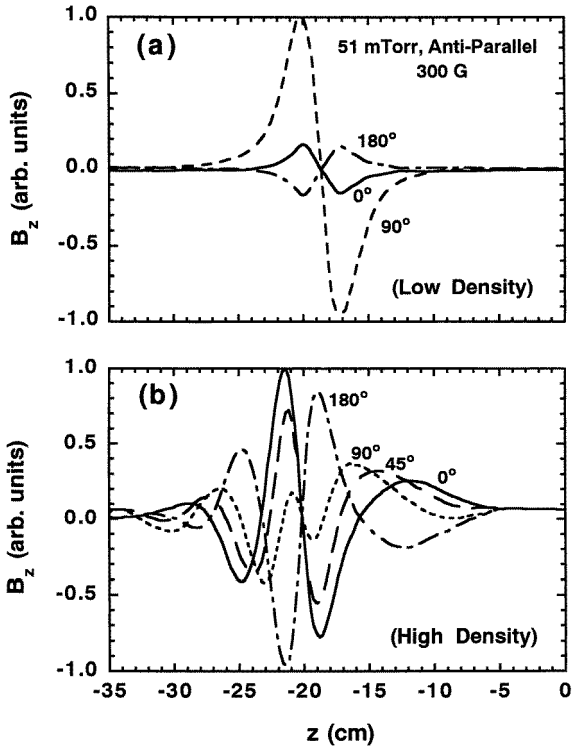

Figure 11. Typical wave patterns of excited magnetic field B_z (axial component) changing the wave phase in (a) low ($\sim 2 \times 10^{11}$ cm^{-3} at $P_{\rm in} = 300$ W) and (b) high ($\sim 10^{13}$ cm^{-3} at $P_{\rm in} = 1500$ W) density regions, with $B = 300$ G (anti-parallel current at $P = 51$ mTorr).

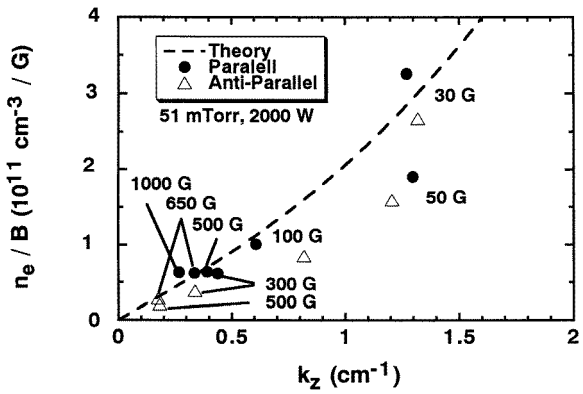

Figure 12. Relationship between $n_{\rm e}/B$ and parallel wavenumber k_z after the density jump, changing the magnetic field B at $P = 51$ mTorr and $P_{\rm in} \sim 2000$ W. Here, closed circles (open triangles) show cases with the use of parallel (anti-parallel) antenna currents, and the dotted curve shows the theoretical dispersion relation of the helicon wave with the first radial mode with azimuthal mode number $m = 0$.

At the low field ($B < 100$ G), helicon and TG waves require the higher k_z component from the dispersion (see the curves in figures 3 and 4). This indicates that there should be an advantage

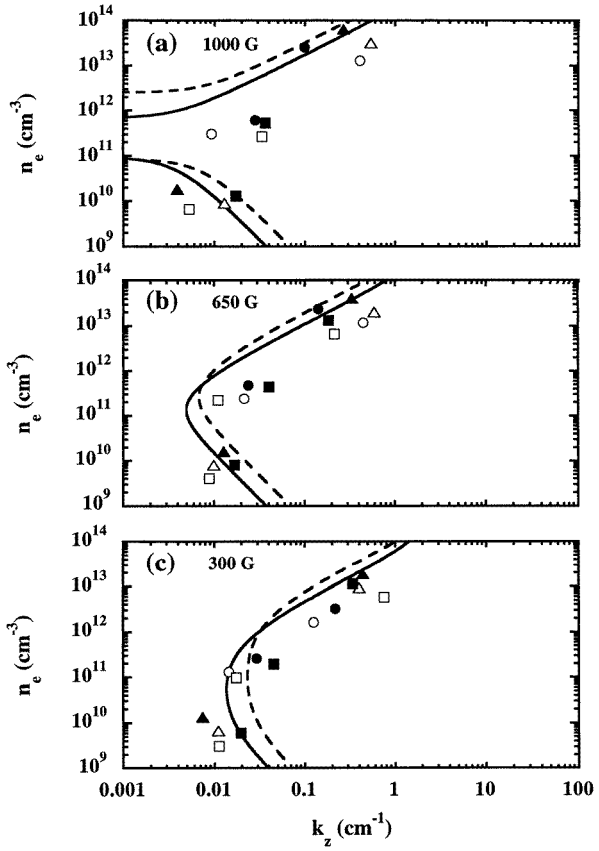

Figure 13. Dependence of electron density n_e on parallel wavenumber k_z under different magnetic fields: (a) 1000 G, (b) 650 G, (c) 300 G, (d) 100 G, (e) 30 G and (f) 5 G. Here, circles (triangles) show cases with parallel antenna currents at $P = 6(51)$ mTorr, and squares show cases with anti-parallel antenna currents at $P = 51$ mTorr. Closed (open) symbols indicate measurements at radius $r = 0$ (2) cm. Solid (dotted) curves denote a theoretical dispersion of the helicon wave with the first (second) radial mode with azimuthal mode number $m = 0$.

to using the antenna with the anti-parallel current direction (see figure 2), but we observed no such advantage. This is because, as will be discussed later, in the low field ($B < 100$ G), neither helicon nor TG waves could be observed, although the dispersion relation after the jump was satisfied on the surface, as shown in figure 12.

The relationship between n_e and k_z for the different magnetic fields is shown in figure 13. For comparison, theoretical curves of the cold-plasma dispersion are shown, using k_{perp} of the first and second radial modes ($m = 0$). It can be seen from figure 13(a) ($B = 1000$ G) that, except for the region of the density gap, measured data fitted well with the TG wave (but on the surface, which will be discussed later) and helicon wave dispersions, both near the edge of $r = 2$ cm as well as in the centre. This density gap did not seem to prevent the plasma from the density jump, as shown in figures 6(a) and 6(b). In the intermediate field (100 G $< B <$ 700 G), most of the data agreed with the theoretical curves, but with the decrease in B, deviations from the curve to the lower k_z direction were enhanced in the low density region. A lower value of k_z means a larger λ (e.g. for $k_z = 0.05$ cm^{-1}, $\lambda = 126$ cm),

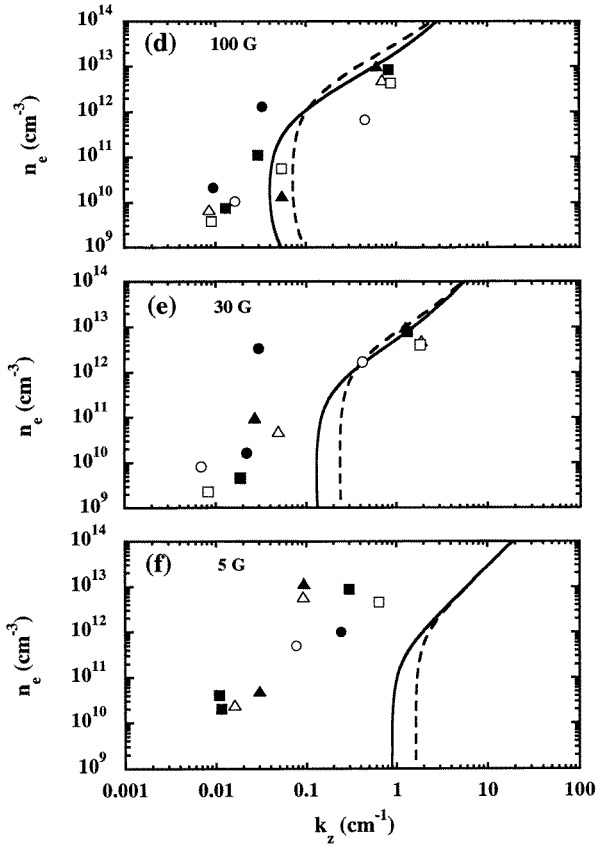

Figure 13. (Continued)

which is longer than the length of the localized wave (nearly standing wave) excited region, typically about 40 cm in total, as mentioned before (see figure 11). For fields less than 100 G, in all the density regions before and after the jump and/or with the high field in the low density region before the jump, the ICP (or CCP in the lower density region) mode prevailed, as will be discussed later. Here, the discrepancy between the theory and experiment was large for $B < 100$ G, even if we consider the density profile effect: as discussed in section 3, the density peaking causes a higher value of k_z with constant n_e from the theoretical dispersion of the TG wave, which means that the curve obtained from the theory became further removed from the experimental values.

Figure 14 shows radial profiles of the amplitude and the phase of excited magnetic fields, azimuthal (B_θ) and axial (B_z) components, for conditions of $P = 51$ mTorr and $B = 500$ G (parallel antenna current) after the density jump. Although there is some scatter, good agreement was found between experiment and helicon wave theory, using the first radial mode, $m = 0$ mode, and a uniform radial n_e profile. In the region of $B > 100$ G, the helicon wave was excited after the density jump, as confirmed by the measurements of these radial structures and the dispersion relation (see figures 12 and 13). However, as B was lowered to less than 100 G, the discrepancy between them was enhanced. The experimentally obtained amplitude and phase did not change very much along the radial direction, even after the jump.

This discrepancy was also found before the jump, regardless of the magnetic field and antenna current directions, which means that ICP formation (or CCP in the lower n_e region with the low B previously mentioned, as shown in figure 6(a)) but not TG wave plasma formation occurred. In contrast to Lho *et al* [32], who found the TG wave in conditions of low n_e and low B with a relatively low k_{perp} (nearly the first radial mode), we did not observe the TG wave in similar regions. This is probably partly due to different conditions, such as filling pressure. Further study is needed using finer radially resolved measurements, especially near the plasma edge region, to detect the TG wave, which has a larger k_{perp} value, under various experimental conditions. Note that the TG wave has an electrostatic rather than an electromagnetic nature.

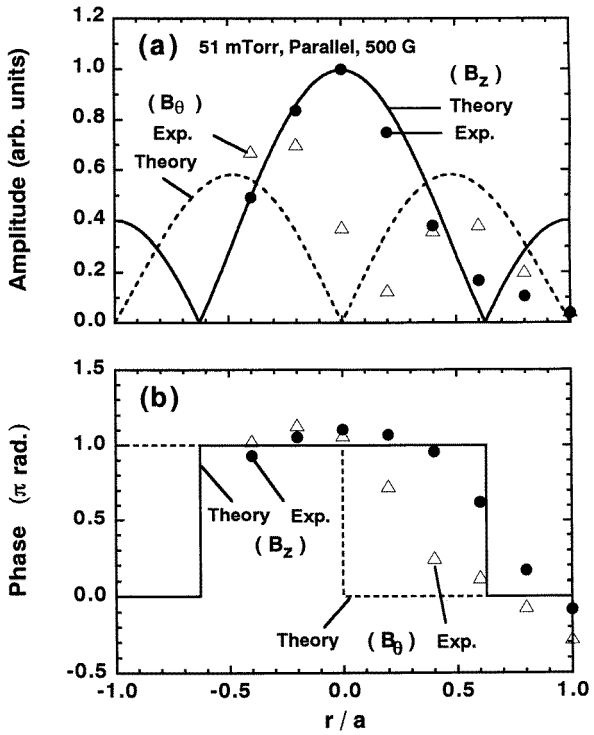

Figure 14. Radial profiles of (a) amplitude and (b) phase of the excited magnetic fields, azimuthal B_θ and axial B_z components, after a density jump with $B = 500$ G, $P = 51$ mTorr and the same antenna current directions. Here, calculation curves of the helicon wave used the first radial mode, azimuthal mode number $m = 0$ and the uniform radial profile of the electron density.

Finally, we will briefly comment on the density jump and the mechanism of the plasma formation. The jump may result from the balance between the non-monotonic variation of the absorbed power and the parameters [20, 33], which we have demonstrated to exercise control, for example n_e versus P_{in}, and the weakly nonlinear functions of the plasma loss. Note that in stellarators, experiments on stepping up density formation in RF plasma were well simulated by a code based on self-consistent numerical modelling [37], and the oscillating nature of the deposited RF power against n_e could also be explained [40]. The plasma production mechanism is still unclear, but the collisional damping may be important at high n_e and in the high P region due to the high collision frequency. Even if the LH wave plays some role in plasma production, which was not found in our experimental conditions, the contribution of this wave is small due to the successful plasma generation in a wide range of magnetic

fields. Enhanced Landau damping [20] is expected theoretically in low B and low n_e sources. However, if electron Landau damping is not important [34], the mode conversion to the TG wave from the helicon wave [33, 34] might be a candidate. Here, we must check whether the density obtained can be sustained or not by this mechanism, since the edge wave power deposition through the mode conversion or direct damping of the TG wave contributes to low production efficiency due to the poor confinement. In addition, the coupling coefficient of helicon and TG waves must be determined. Needless to say, the role of the near field, such as an inductive field, must also be considered.

5. Conclusions

Density jumps in a helicon plasma source were successfully demonstrated by changing the antenna wavenumber spectrum (two loops with parallel and anti-parallel current directions) in addition to P (6 and 51 mTorr) and B (from 0 to 1000 G). For the anti-parallel antenna case, P_{th} was larger than in the parallel case, regardless of B and P, and P_{th} became larger with the increase in B in both cases. These features could be explained by the dispersion relation.

The helicon wave plasma was observed after the jump in the case of the high field (>100 G), while ICP (or CCP in the lower density) was found in the case of the low field (<100 G) regardless of the density region or with the high field (>100 G) before the jump. No indication of a major role of the LH or TG waves was observed in our experimental conditions.

Acknowledgment

We would like to thank Professor Y Kawai for his continuous encouragement and Dr M D Bowden for checking the English.

References

[1] Boswell R W 1984 *Plasma Phys. Control. Fusion* **26** 1147
[2] Chen F F 1991 *Plasma Phys. Control. Fusion* **33** 339
[3] Chen F F 1996 *Phys. Plasmas* **3** 1783 and references therein
[4] Shinohara S 1997 *Japan. J. Appl. Phys.* **36** 4695 and references therein
[5] Komori A, Shoji T, Miyamoto K, Kawai J and Kawai Y 1991 *Phys. Fluids* B **3** 893
[6] Loewenhardt P K, Blackwell B D, Boswell R W, Conway G D and Hamberger S M 1991 *Phys. Rev. Lett.* **67** 2792
[7] Shoji T, Sakawa Y, Nakazawa S, Kadota K and Sato T 1993 *Plasma Sources Sci. Technol.* **2** 5
[8] Yasaka Y and Hara Y 1994 *Japan. J. Appl. Phys.* **33** 5950
[9] Chen F F, Hsieh M J and Light M 1994 *Plasma Sources Sci. Technol.* **3** 49
[10] Shamrai K P and Taranov V B 1994 *Plasma Phys. Control. Fusion* **36** 1719
[11] Fischer B, Krämer M and Enk Th 1994 *Plasma Phys. Control. Fusion* **36** 2003
[12] Shinohara S, Miyauchi Y and Kawai Y 1995 *Plasma Phys. Control. Fusion* **37** 1015
[13] Shinohara S and Kawai Y 1995 *Japan. J. Appl. Phys.* **34** L1571
[14] Ellingboe A R, Boswell R W, Booth J P and Sadeghi N 1995 *Phys. Plasmas* **2** 1807
[15] Light M, Sudit I D, Chen F F and Arnush D 1995 *Phys. Plasmas* **2** 4094
[16] Shinohara S, Miyauchi Y and Kawai Y 1996 *Japan. J. Appl. Phys.* **35** L731
[17] Shinohara S, Takechi S and Kawai Y 1996 *Japan. J. Appl. Phys.* **35** 4503
[18] Ellingboe A R and Boswell R W 1996 *Phys. Plasmas* **3** 2797
[19] Cho S 1996 *Phys. Plasmas* **3** 4268
[20] Kamenski I V and Borg G G 1996 *Phys. Plasmas* **3** 4396
[21] Shamrai K P and Taranov V B 1996 *Plasma Sources Sci. Technol.* **5** 474
[22] Shamrai K P, Pavlenko V P and Taranov V B 1997 *Plasma Phys. Control. Fusion* **39** 505
[23] Shinohara S, Takechi S, Kaneda N and Kawai Y 1997 *Plasma Phys. Control. Fusion* **39** 1479

[24] Chen F F, Jiang X, Evans J D, Tynan G and Arnush D 1997 *Plasma Phys. Control. Fusion* **39** A411
[25] Borg G G and Kamenski I V 1997 *Phys. Plasmas* **4** 529
[26] Sakawa Y, Shoji T, Takino T, Kuroki Y and Shimura K 1997 *Proc. 1996 Int. Conf. on Plasma Phys. (Nagoya, 1996)* vol 2 (Nagoya: Japan Society of Plasma Science and Nuclear Fusion Research) p 1334
[27] Yun S M, Kim J H and Chang H Y 1997 *J. Vac. Sci. Technol.* A **15** 673
[28] Yun S M and Chang H Y 1998 *Phys. Lett.* **248** 400
[29] Shinohara S, Kaneda N and Kawai Y 1998 *Thin Solid Films* **316** 139
[30] Chen R T S and Hershkowitz N 1998 *Phys. Rev. Lett.* **80** 4677
[31] Arnush D and Chen F F 1998 *Phys. Plasmas* **5** 1239
[32] Lho T, Hershkowitz N, Miller J, Steer W and Kim G H 1998 *Phys. Plasmas* **5** 3135
[33] Shamrai K P 1998 *Plasma Sources Sci. Technol.* **7** 499
[34] Chen F F and Blackwell D D 1999 *Phys. Rev. Lett.* **82** 2677
[35] Cheung P Y, Donovan S and Wong A Y 1998 *Phys. Rev. Lett.* **61** 1360
[36] Hopwood J 1992 *Plasma Sources Sci. Technol.* **1** 109
[37] Moiseenko V E, Plyusnin V V, Lyssoivan A I, Volkov E D, Nagarov N I, Kasilov S V and Litvinov A P 1996 *Proc. 23rd Eur. Conf. on Controlled Fusion and Plasma Physics (Kiev, 1996)* vol 20C (Geneva: EPS) part II, p 926
[38] Stix T H 1992 *Waves in Plasmas* (New York: American Institute of Physics)
[39] Shinohara S and Soejima T 1998 *Plasma Phys. Control. Fusion* **40** 2081
[40] Moiseenko V E, Lyssoivan A I, Kasilov S V and Plyusnin V V 1995 *Fusion Eng. Design* **26** 203